ORIGINAL PAPER

On the enhanced post-impoundment seismicity in the Three Gorges Reservoir region, China

Kalpna Gahalaut[1] · Rajesh Rekapalli[1]

Abstract

Since the impoundment of the Three Gorges Reservoir (TGR) in the year 2003 in central China, the region is experiencing enhanced seismic activity. The enhanced seismicity after the TGR impoundment has been reported to be associated with several factors, e.g., Karst collapse, mine collapse, chemical effects due to water percolation, and reservoir-assisted shear failure on the mapped and seismological faults. Here in this article, we explore in detail the role of reservoir impoundment in mobilizing the nearby faults leading to increase in post-impoundment seismicity of the region. For this purpose, reservoir induced stress, pore pressure and their influence on subsurface faults, in terms of fault stability, are calculated to explore the role of TGR in inducing shear failure on the earthquake causative faults. Our analysis suggests that some of the areas of enhanced post-impoundment seismicity can be explained by the shear failure due to the reservoir impoundment. But a large region, despite being under the unfavourable influence of reservoir induced stress, also exhibit enhanced post-impoundment seismicity. Even the pore pressure due to the reservoir impoundment is not enough to mobilize these faults in these unfavourable regions. An extremely high pore pressure or some other mechanism, involving fluid interaction with rock mass due to the reservoir impoundment, is required to explain the enhanced seismicity in such regions. We suggest that dissolution and reduced cohesion in the Karst–Carbonate rocks present in the region also assisted in the enhancement of the post-impoundment seismicity. These post-impoundment earthquakes may be termed as fluid-assisted earthquakes in the TGR region rather than earthquakes linked with reservoir induced shear failure. Further, some of the post-impoundment earthquakes of relatively large magnitude which occurred in the region of pre-impoundment seismicity could be purely tectonic in nature and not influenced by the reservoir impoundment. Thus, we suggest that along with the TGR induced shear failure, various other factors also play significant role in the increase of post-impoundment seismicity.

**Keywords** Three Gorges Reservoir · Fault stability · Shear failure · Karst-Carbonate

✉ Rajesh Rekapalli
  rekapalli@gmail.com

1   CSIR- National Geophysical Research Institute, Uppal Road, Hyderabad 500007, India

1 Introduction

Three Gorges hydroelectric dam on the Yangtze River, Hubei province China (Fig. 1), is seismologically very well monitored project. The impoundment of the Three Gorges Reservoir (TGR) started in May 2003. In 1958, well before the impoundment, the China Earthquake Administration (CEA) started to establish seismic monitoring network in the TGR region (Yao et al. 2017) which is now running continuously for ∼ 63 years along with some temporary and intermittent seismic networks. The CEA network has been upgraded in four stages. From 1958 to 1996, only 5 seismic stations operated. A transitional seismic network was in operation from 1997 to 2000 consisting of 8 seismic stations. From 2001 to 2011, a network of 24 permanent stations operated with short-period seismometers, which was upgraded in 2012 when along with 19 short-period seismometers, three broadband seismometers were deployed (Zhang et al. 2019). Various other temporary networks were also in operation intermittently in the TGR region after the impoundment.

Broad geological features along with the major mapped faults in the TGR region are shown in Fig. 1. Huangling Anticline (HLA) consists of the metamorphic and volcanic fractured unit, and Zigui basin (ZGB) consists of clastic unit (Yi et al. 2012). Apart from these two units, most of the area under consideration consists of heavily Karstic unit, mainly composed of limestone and dolomite limestone, and weak Karstic unit, mainly composed of limestone interrupted by mud and shale (Yi et al. 2012).
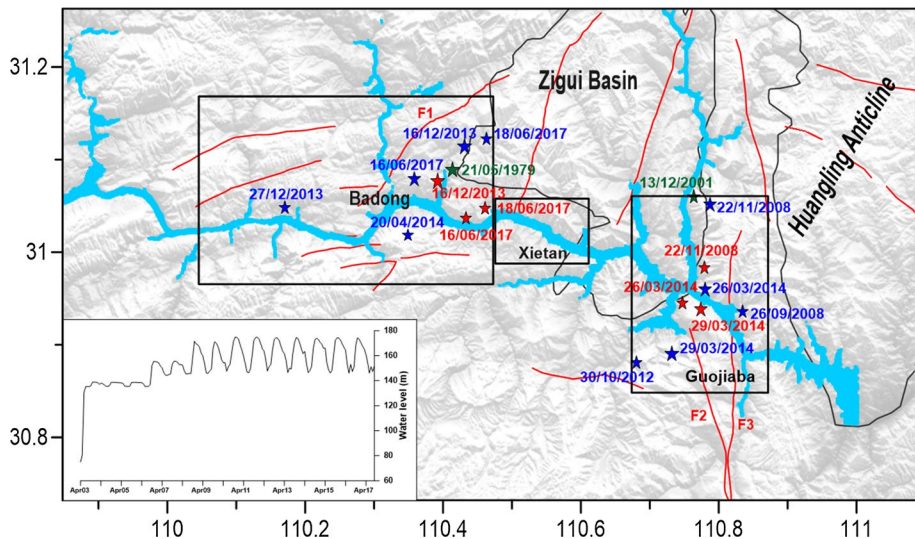
Fig. 1 Broad primary geological features along with the mapped major faults (Hua et al. 2013) in the TGR region on the grey scale topography map. Some major faults are marked as F1(Gaoqiao fault, Hua et al. 2013), F2 (Xiannvshan fault, Hua et al. 2013) and F3 (Jiuwanxi fault, Hua et al. 2013). Three rectangles represent the three zones, namely Badong, Xietan and Guojiaba, where post-impoundment seismicity is reported. Temporal variation of water load at the dam site is shown on the left bottom inset. Six red stars indicate earthquake epicenters recorded by CEA of $M \geq 4.0$ in the region (details are given in Table 1) along with earthquakes of $M \geq 4.0$ reported by ISC and ISC-EHB (Table 1) before (green filled star) and after (blue filled star) TGR impoundment. Earthquakes from different agencies with same date are shown here with different colour and symbol. The impounded reservoir is shown by the blue colour

Various studies have been done on post-impoundment seismicity by using data from the temporary and permanent seismic networks in the TGR region. A common conclusion from all the published studies was that the seismicity increased many folds in the TGR region after the reservoir impoundment in 2003, which otherwise was considered a region of very low seismicity. Yi et al. (2012) analysed the seismicity from May 2003 to December 2009 and associated it with the abandoned coal and copper mines, Karst, and also with a few nearby faults in the region. Hua et al. (2013) observed that seismicity derived from a temporary network, which was in operation from March 2009 to July 2010, was distributed in various clusters in all three zones rather than along faults and fractures. Based on the low-stress drop associated with the small magnitude earthquakes, Hua et al. (2013) suggested a significant role of fluid on the enhanced post-impoundment seismicity. Further, they suggested that the seismicity might not be controlled by faults, but the faults might have helped as conduits for water flow. Wen-Tao et al. (2010) (paper in Chinese with abstract in English) notified the distribution of 2995 earthquakes in clusters, recorded from a local network from March to December 2009. They classified earthquakes in the TGR region due to the collapse caused by softening of discontinuities by the water permeation into Karst-Carbonate strata and also due to mining. Zhang et al. (2017) on the basis of statistical analysis, using earthquake catalogue of the period 2003 to 2009, associated the Badong zone seismicity with the Karst collapse, fault slip and landslides; Xietan zone seismicity with the mine collapse; and Guojiaba zone seismicity with the fault slip due to change in stress and pore pressure because of the TGR impoundment. Zhang et al. (2018) analysed the Guojiaba zone seismicity for the period from September 2008 to September 2017 and suggested that the combined effect of change in stress and pore pressure, and chemical effects of water due to the TGR impoundment played an important role in the enhancement of post-impoundment seismicity. Zhang et al. (2016) performed the fault stability analysis for the December 16, 2013 Badong zone earthquake and November 22, 2008 Guojiaba zone earthquake, and inferred that both the earthquakes were influenced by the reservoir impoundment and occurred due to shear failure on their respective fault planes.

Different views, as discussed above, about the genesis of the enhanced post-impoundment seismicity in the TGR region, i.e., Karst collapse, mine collapse, chemical effects due to water percolation, and also reservoir-induced shear failure on the mapped faults, prompted us to write this article. We are of the view that whenever there is an increase in seismicity after the impoundment of a hydroelectric reservoir, the first step should be to explore the relationship between the reservoir impoundment and enhancement of seismicity through the physical mechanism of RTS. The purpose of such an analysis is to investigate whether reservoir impoundment mobilizes the shear/frictional failure on the pre-existing faults of the area. Here, we use the seismicity data, reservoir water level data and earthquake focal mechanisms published in various articles. Accuracy and completeness in earthquake catalogues are discussed in the respective original articles (e.g., Zhang et al., 2018; Huang et al., 2018) and hence for the sake of brevity, it has been avoided here. Nevertheless, we have cross-checked it from various published articles and found it consistent. We have taken the locations of earthquakes ($M \geq 4.0$) given by CEA as reported by earlier workers in their published articles (given in Table 1). For smaller magnitude earthquakes exact location of the individual earthquake is not considered, but the entire seismicity is divided into three distinct zones based on the earthquake clustering, as has also been done by earlier workers (Fig. 4 of Yi et al. 2012; Fig. 3 of Hua et al. 2013; Fig. 1 of Zhang et al. 2017; Fig. 2 of Zhang et al. 2018). We analyse the enhanced post-impoundment seismicity of the TGR region in the ambit of the physical mechanism of RTS. For this purpose, we calculate reservoir-induced stress and pore pressure and fault stability in the region and assess the role of TGR in triggering shear failure on the

Table 1 Details of $M \geq 4.0$ Earthquakes in the TGR region as given by China Earthquake Administration (CEA, Zhang et al. 2018) and International Seismological Center (ISC) and ISC-Engdahl-van der Hilst-Buland (ISC-EHB) earthquake catalogues

No.	Date	CEA				ISC-EHB				Zone
		Long	Lat	M	Agency	Long	Lat	M	Agency	
1	21.05.1979					110.41	31.08	5.0	ISC-EHB	Badong
2	13.12.2001					110.76	31.06	4.5	ISC	Guojiaba
3	26.09.2008					110.83	30.93	4.2	ISC	Guojiaba
4	22.11.2008	110.77	30.98	4.1	CEA	110.78	31.05	4.6	ISC	Guojiaba
5	30.10.2012					110.68	30.88	4.1	ISC	Guojiaba
6	16.12.2013	110.39	31.07	5.1	CEA	110.43	31.11	5.1	ISC-EHB	Badong
7	27.12.2013					110.16	31.04	4.1	ISC	Badong
8	27.03.2014	110.74	30.94	4.3	CEA	110.78	30.96	4.6	ISC-EHB	Guojiaba
9	30.03.2014	110.77	30.93	4.7	CEA	110.73	30.89	5.0	ISC-EHB	Guojiaba
10	20.04.2014					110.34	31.01	4.0	ISC	Badong
11	16.06.2017	110.43	31.03	4.3	CEA	110.35	31.07	4.6	ISC	Badong
12	18.06.2017	110.46	31.04	4.1	CEA	110.46	31.12	4.3	ISC	Badong

earthquake causative faults. Then, we evaluate the role of other factors, mentioned above in various studies, in the occurrence of these earthquakes.

2 Stress and pore pressure due to the reservoir impoundment and fault stability analysis

Fault stability analysis is performed to analyse the effect of stress and pore pressure induced by the impoundment of the TGR on seismogenic faults of the region. To calculate stress and pore pressure due to the reservoir impoundment, the water load is simulated by considering the actual geometry of the TGR (from Google Earth). The extent of the TGR is approximated by 5000 cuboids, each having a uniform water load which is assigned according to the bathymetry under the reservoir (from Google Earth). The total assigned water load of the TGR is constrained so that the total volume of the simulated water load is equal to the actual water volume in the reservoir for a maximum 175 m water head at the dam site (from the MSL). The temporal variation of water level at the dam site (digitized from Fig. 3 of Zhang et al., 2018), shown in Fig. 1, governs the temporal variations of water load in each considered cuboid. Thus, simulated spatio-temporal reservoir water load is used to calculate six independent stress components using the Boussinesq equations (Jaeger et al. 2007). These stress components are resolved into shear and normal direction of fault plane to derive the change in shear ($\Delta\tau$) and normal ($\Delta\sigma$) stresses due to the reservoir impoundment. Pore pressure (ΔP) is computed by solving the following inhomogeneous diffusion equation,

$$c\nabla^2(\Delta P) = \frac{\partial}{\partial t}\left((\Delta P) - B\left(\frac{\Delta\theta}{3}\right)\right) \tag{1}$$

here θ is the sum of normal stresses, B is the Skempton's coefficient and c is the hydraulic diffusivity. Pore pressure is calculated by using Green's function approach of Gahalaut

(2021) and Kalpna and Chander (2000). Change in fault stability without pore pressure (ΔS) and with pore pressure (ΔS_p) due to the reservoir impoundment is calculated considering the Coulomb-Mohr failure criterion of frictional/shear failure of earthquake occurrence (King et al. 1994; Hardebeck et al. 1998; Scholz 1990),

$$\Delta S_P = \Delta\tau - \mu(\Delta\sigma - \Delta P) = (\Delta\tau - \mu\Delta\sigma) + \mu\Delta P = \Delta S + \mu\Delta P \qquad (2)$$

here μ is the coefficient of friction. Positive $\Delta\tau$, negative $\Delta\sigma$ and, positive ΔS and ΔS_p on a fault plane indicate the favourable role of reservoir impoundment in mobilising the considered fault plane towards failure. ΔP always mobilizes the faults towards failure. We have assumed that all earthquakes in the region occurred due to shear failure (Eq. 2) on their respective fault planes.

We did a detailed fault stability analysis for the Badong and Guojiaba zone seismicity. The Xietan zone seismicity has been related to mine collapse (Yi et al. 2012; Zhang et al. 2017) and thus is not analysed in this study. The epicenters of six earthquakes of $M \geq 4.0$ in the TGR region are shown in Fig. 1 by the red star (Table 1, Zhang et al. 2018). The earthquakes of $M \geq 4.0$ (Table 1) reported by the International seismological center (ISC) and ISC-Engdahl-van der Hilst-Buland (ISC-EHB) before and after TGR impoundment are also shown with green and blue color stars, respectively, in Fig. 1.

2.1 Analysis for Badong zone

The fault plane solutions (FPS) of three Badong zone earthquakes of $M \geq 4.0$ (dated December 16, 2013, June 16, 2017 and June 18, 2017) used in the present analysis are given in Table 2. For Badong zone earthquakes, we consider the eastward dipping plane as the fault plane, based on orientation and dip of the geological faults present in the area (Yi et al. 2012) and also based on the depth section of seismicity of the zones (Zhang et al. 2016, 2019, 2018; Huang et al. 2018). The depth of these three earthquakes varies from 4 to 6 km (Zhang et al. 2019) and in general Badong zone seismicity occurs between ~2–10 km depth (Huang et al. 2018; Zhang et al. 2019). Thus, we performed all the calculations at three depths, namely 2 km, 6 km and 10 km. We have considered three values of c i.e., 0.1 m²/s, 1.0 m²/s and 10 m²/s to cover the full range of c as given by Talwani et al. (2007) for triggered earthquake cases. The value of μ is considered as 0.4. A nominal value of B is considered as 0.7 (Talwani et al., 2007). Table 3 shows the values of $\Delta\tau$, $\Delta\sigma$, ΔP, ΔS and ΔS_P at the location and epoch (Table 1) of the three earthquakes of Badong zone for

Table 2 Available fault plane solutions (FPS) of earthquakes by CEA given in Table 1

Zone	Date	FPS			Source
		Strike	Dip	Rake	
Badong	16.12.2013	73	58	168	Huang et al. (2018)
		70	62	172	Zhang et al. (2019)
		74	56	−178	Zhang et al. (2016)
	16.06.2017	67	53	170	Zhang et al. (2019)
	18.06.2017	62	61	180	Zhang et al. (2019)
Guojiaba	22.11.2008	213	81	110	Zhang et al. (2016)
	27.03.2014	143	60	1	Yao et al. (2017)
	30.03.2014	226	54	155	Yao et al. (2017)

the respective FPS given in Table 2, for $\mu = 0.4$ and $z = 6$ km. As the results do not differ much at other depths, they are tabulated in Table S1 and S2 for z = 2 km and 10 km. For all the three considered fault planes for December 16, 2013 earthquake (Table 2), resolved $\Delta\tau$ is negative, $\Delta\sigma$ is positive, and both ΔS and ΔS_P are negative (Tables 3, S1 and S2) at all depths and for the full range of c. At the epoch and epicenter of June 16, 2017 earthquake, the estimated $\Delta\tau$ and $\Delta\sigma$ are positive, and ΔS is negative at all depths over the complete range of c (Tables 3, S1 and S2). For full range of c, ΔS_P is positive at 6 km and 10 km depth (Tables 3, S2) but negative at 2 km depth (Table S1). At the epoch and epicenter of 18 June 2017 earthquake, the computed $\Delta\tau$, $\Delta\sigma$ are positive for all depths (Tables 3, S1 and S2), and ΔS and ΔS_P are positive at 6 km and 10 km (Tables 3 and S2) but negative at 2 km depth (Table S1), over the full range of c.

For more clarity and to understand the seismicity of the Badong zone as a whole, results are shown in plan-view also (Fig. 2) at the epoch of December 16, 2013 for the fault plane as considered by Zhang et al. (2016) in their study. For brevity, the results for $c = 1.0$ m²/s only are shown in the main text and the results of ΔS_P for the other two values (0.1 m²/s and 10 m²/s) are shown in the supplementary (Figures S1 and S2). We also performed calculations for other fault planes given in Table 2, but not shown here as the results do not differ much from the above. Although the results shown in Figs. 2, S1 and S2 are calculated at a particular epoch of the earthquake occurrence, they can be generalized for the other earthquakes of similar focal mechanisms but occurred at different epochs, at least qualitatively. This is valid because each quantity ($\Delta\tau$, $\Delta\sigma$, ΔP, ΔS, and ΔS_P) retain its sign at every location for changes in the TGR water level (Fig. 1, inset) from its minimum (135 m) to maximum (175 m) for the fault plane. It implies that the zero value contour does not change its position significantly in these figures for a fault plane and the positive and negative regions for all the calculated quantities remain positive and negative, irrespective of the time of occurrence of earthquake after the reservoir impoundment. To validate it, the temporal variations of all the components are shown in Fig. 3 for $z = 6$ km and 10 km and for $c = 1.0$ m²/s at the location of the December 16, 2013 earthquake by considering the same fault plane as considered in Fig. 2 for the whole reservoir water level time series, which clearly shows that qualitatively all the components retain their sign (positive or negative) in time.

2.2 Analysis for Guojiaba zone

We analysed the three Guojiaba zone earthquakes having $M \geq 4.0$ (dated November 22, 2008, March 27, 2014 and March 30, 2014). The details regarding FPS of the three earthquakes are given in Table 2. For Guojiaba zone earthquakes, we consider westward dipping plane as the fault plane based on the orientation and dip of geological faults present in the area (Yi et al. 2012) and depth section of seismicity of the zones (Zhang et al. 2016, 2019, 2018; Huang et al. 2018). All other parameters (z, c and B) for the analysis are the same as considered for the Badong zone analysis. Table 3 shows the values of $\Delta\tau$, $\Delta\sigma$, ΔP, ΔS, and ΔS_P at a particular location and epoch of the three earthquakes of Guojiaba zone (Table 1) for $\mu = 0.4$ and $z = 6$ km for their respective fault plane given in Table 2. For brevity, the tables for $z = 2$ km and 10 km are shown in the supplementary (Table S1 to S2). At the epoch and epicenter of November 22, 2008 earthquake, resolved $\Delta\tau$ is negative, $\Delta\sigma$ is positive and, ΔS and ΔS_P both are negative (Table 3, S1 and S2) at all depths, for the full range of c. At the epoch and epicenter of the March 27, 2014 earthquake, $\Delta\tau$ and $\Delta\sigma$ are positive (Tables 3, S1, S2) for all considered depth and c values. For all c values, ΔS and ΔS_P are

Table 3 Results of fault stability analysis for the respective FPS of earthquakes given in Table 2 for z = 6 km

Zone	Date	z = 6 km		ΔP (kPa)			$\mu = 0.4$			
		$\Delta\tau$ (kPa)	$\Delta\sigma$ (kPa)				ΔS (kPa)	ΔS_p (kPa)		
				$c = 0.1$ m²/s	$c = 1.0$ m²/s	$c = 10$ m²/s		$c = 0.1$ m²/s	$c = 1.0$ m²/s	$c = 10$ m²/s
Badong	16.12.2013	− 12.1	40	16.7	23.5	13.6	− 28.1	− 21.4	− 18.7	− 22.7
		− 9.9	35.6				− 24.1	− 17.5	− 14.8	− 18.7
		− 5.9	42.2				− 22.8	− 16.1	−13.4	− 17.3
	+16.06.2017	2.6	14.9	21.9	28.6	13.3	− 3.4	5.3	8.0	1.9
	18.06.2017	4	18.4	22	28.9	13.3	− 3.8	5.4	8.2	1.9
Guojiaba	22.11.2008	− 15.9	25.3	14.3	28.6	16.6	− 26.0	−20.3	− 14.6	− 19.4
	27.03.2014	11.5	15.7	31.7	46.5	21.9	5.2	17.9	23.8	13.9
	30.03.2014	− 12.7	52.7	25.8	39.4	20.9	− 33.8	−23.5	− 18.1	− 25.4

Fig. 2 Results (colour image and zero value contour) of resolved stress ($\Delta\tau$ and $\Delta\sigma$), pore pressure (ΔP) ▶ and fault stability (ΔS and ΔS_P) for $c = 1.0$ m²/s are shown in panels from (a) to (e) at three depths, for December 16, 2013 Badong zone earthquake fault plane having strike $= 74°$, dip $= 56°$ and rake $= -- 178°$. All the results are in kPa. The white star indicates the earthquake whose time epoch is considered for calculations (Table 2). Other five earthquake locations (Table 2) are shown by white star. In all the panels red and green colours show the favourable and opposing mobilization of faults, respectively

positive at 6 km (Table 3) and 10 km depths (Table S2). At 2 km depth, ΔS is negative (Table S1) for the full range of c values but ΔS_P is negative for $c = 10$ m²/s and positive for other two lower values of c. At the epoch and epicenter of the March 30, 2014 earthquake, the estimated $\Delta\tau$ is negative, $\Delta\sigma$ is positive and, ΔS and ΔS_P both are negative (Tables 3, S1 and S2) at all depths, for the full range of c.

The results shown in plan-view (Figs. 4, 5, 6) at the respective epoch of the three Guojiaba Zone earthquakes for their respective fault plane (Table 2) provide more clear understanding. For brevity, results for $c = 1.0$ m²/s only are shown in the main text and also ΔP are not shown because it will be always positive in every case and are similar to Fig. 2c. Results of ΔS_P for the other two values (0.1 m²/s and 10 m²/s) are shown in the supplementary (Figure S3–S8). The temporal variations of all the components are plotted (Fig. 7) at the location of the November 22, 2008 earthquake for the same fault plane as considered in Fig. 4 to show that all the components retain their sign (positive or negative) in time. Thus, the results shown for the particular epoch (Figs. 4, 5,6) can be generalized for the qualitative interpretation of all the earthquakes that occurred at any time of reservoir impoundment with similar focal mechanisms. The temporal variation calculations are done for the other two Guojiaba Zone earthquakes also but are not shown here because of the same features of the calculated quantities as discussed in Fig. 7.

3 Discussion

3.1 Implications of fault stability analysis

We discuss the implications of considering a homogeneous poroelastic medium and associated uncertainties in the earthquake parameters on the computations, results and inferences. The consideration of homogeneous poroelastic half-space mainly influences the pore pressure changes (ΔP) and thereby associated fault stability (ΔS_P). We acknowledge that the actual representation of the region and the process requires consideration of heterogeneous medium. However, this also requires knowledge of several parameters governing the medium, fault zones and other heterogeneities. In the absence of information on these parameters, we need to consider several simulations. Gahalaut and Gupta (2008) simulated the pore pressure in a heterogeneous medium that consists of a fault with higher c value surrounded by a medium having comparatively lower c value. They suggested that in this case, the pore pressure is high in and around the considered faults, but even this high pore pressure is less than the pore pressure when a homogeneous poroelastic medium has higher c value that is the same as of fault is considered. In view of the above, we undertook a simple modeling approach and performed our analysis over the full range of c (i.e., 0.1 m²/s to 10 m²/s). In that way, these simulations become the end member calculations. Although the consideration of higher c values in simulating stability of faults renders overestimation of pore pressure, interestingly even these end-member computations suggest that the region of stabilization and destabilization remain stationary within the permissible range of c and for
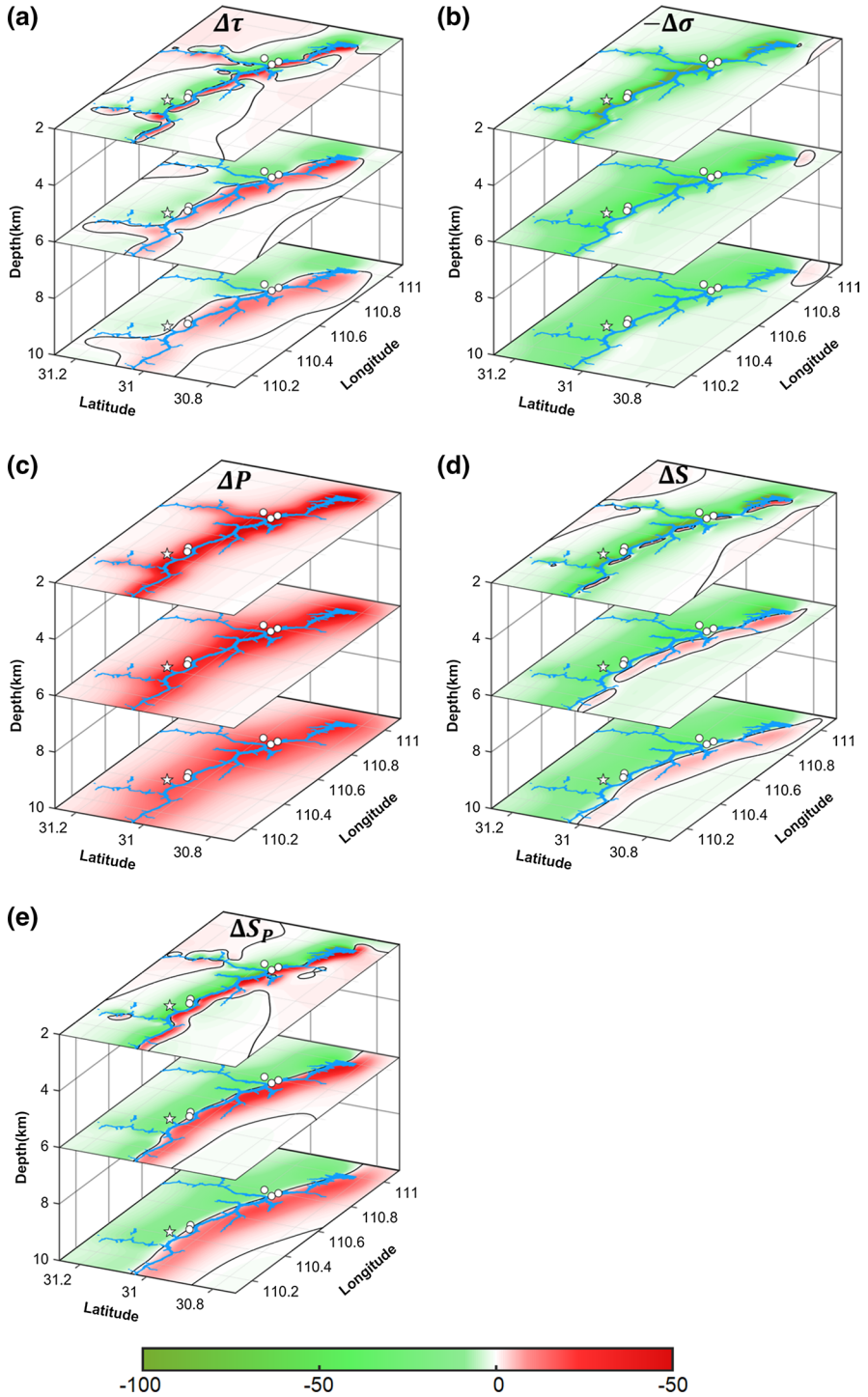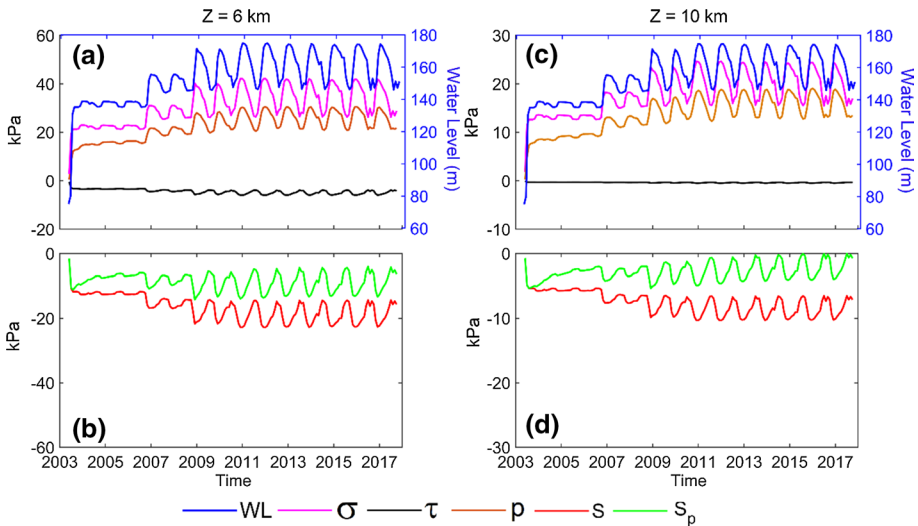
Fig. 3 Temporal variation of $\Delta\tau$, $\Delta\sigma$, ΔP, ΔS and ΔS_P (in kPa) with reservoir water level (WL) at the dam site for the same fault plane as considered in Fig. 2 and at the location (Table 1) of December 16, 2013 Badong zone earthquake for $c = 1.0$ m^2/s

the given focal mechanism solutions. This suggests that the qualitative results and associated inferences derived in our study are quite justifiable. We hope that the availability of open data and constraints on the parameters in the future will help to consider more complex and heterogeneous medium. We acknowledge that there could be errors/uncertainties in the earthquake parameters (e.g., hypocentral location and focal mechanisms). To address this issue, we have considered all possible depth ranges and have considered all the available fault plane solutions. For the consideration of errors in epicentral location, other than reporting results at the epicentre (Table 3, S1 and S2), results in plan-view are also shown (Figs. 2, 4, 5, 6 and S1–S8) which are interpreted in the following paragraph.

For the Badong zone, most of the seismicity lies north of the reservoir (Fig. 1 of Zhang, et al. 2017; Fig. 2 of Zhang et al. 2018; Fig. 4 of Huang et al. 2018; Fig. 4 of Yi et al. 2012) whereas per our analysis even $\Delta\tau$ is negative (Fig. 2a) and even high pore pressure is not able to mobilize faults towards failure as ΔS_P is also negative (Fig. 2e, S1 and S2) to the north of the reservoir. It may be noted that for a case where $\Delta\tau$ is negative, only very large pore pressure can mobilize fault towards failure. Further, we suggest that shear/frictional failure cannot be ruled out completely for some of the earthquakes of the Badong zone, specifically in the case of higher magnitude earthquakes that lie north of the reservoir and for a few earthquakes which lie south of the reservoir (as ΔS_P is positive here). We opine that higher magnitude earthquakes, e.g., the December 16, 2013 Badong zone earthquake (M 5.1) may be associated with the geological fault marked as F1 in Fig. 1. But whether it would be called a reservoir-triggered earthquake, is still an open debate, as the change in shear stress, normal stress and fault stability due to the reservoir impoundment are insufficient to mobilize the fault towards failure to the north of the reservoir (Fig. 2). In our view, December 16, 2013 might be a natural tectonic earthquake of the region, as the epicenter of the pre-impoundment earthquake of May 21, 1979 (M 5.0) is also located in the Badong zone (Fig. 1). Yao et al. (2017) also indicated that higher magnitude earthquakes are not correlated with water level variations in the TGR region. In short, Badong zone
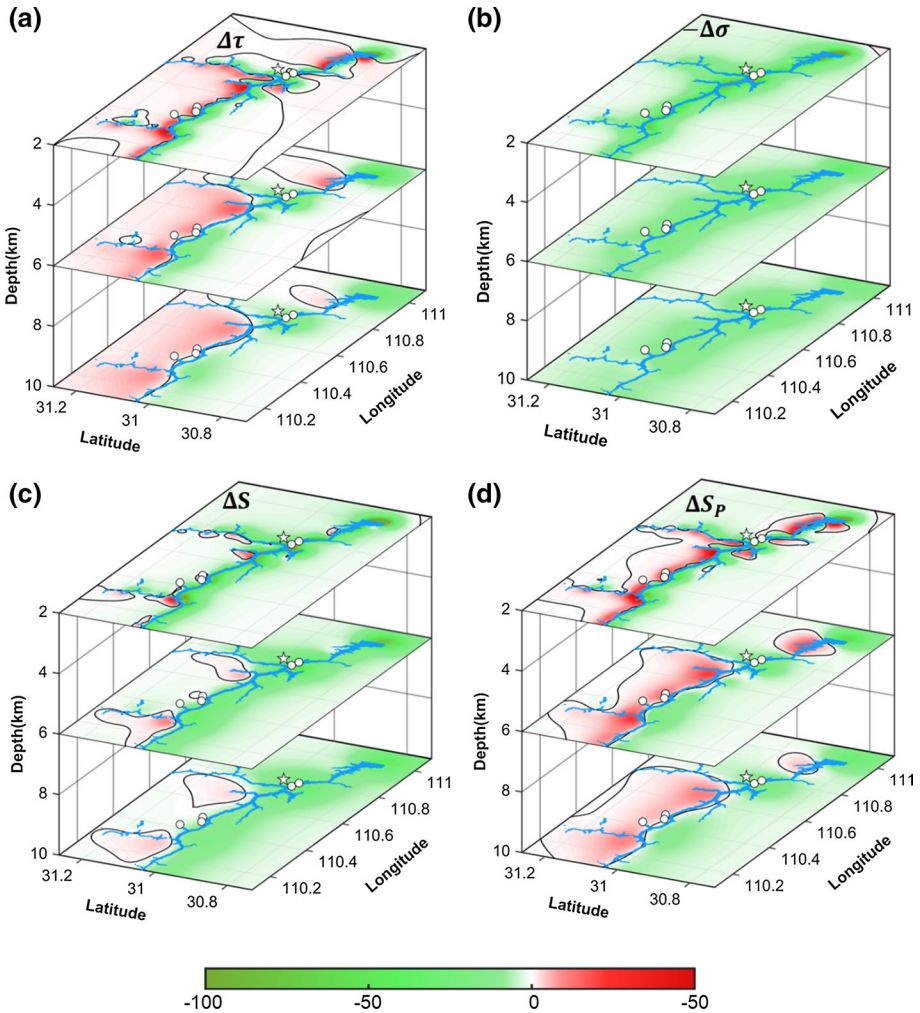
Fig. 4 Same as Fig. 2 but for November 22, 2008 Guojiaba Zone earthquake having strike = 213°, dip = 81° and rake = 110°

post-impoundment seismicity is primarily fluid-driven and/or the ambient tectonic stresses play a major role in the occurrence of post-impoundment earthquakes. There is also a possibility that other factors, as discussed in the next section might have also played some role in the enhancement of the post-impoundment seismicity in this zone.

For the Guoziaba zone earthquakes, fault stability analysis is bit complicated as the reported seismicity in this zone is distributed both to the north and south of the reservoir (Fig. 1 of Zhang, et al. 2017; Fig. 2 of Zhang et al. 2018; Fig. 4 of Yi et al. 2012). Also, fault plane solutions (Table 2) of the earthquakes in this zone have large variations. For November 22, 2008 type of fault planes, $\Delta\tau$ is negative (Fig. 4a). Even the induced pore pressure is not able to mobilize faults towards failure, as ΔS_P too is negative (Fig. 4d, S3 and S4) in the entire zone, whether to the north or south of the reservoir. We suggest that the earthquakes which occurred on this type of fault plane might have been associated with the geological fault marked as
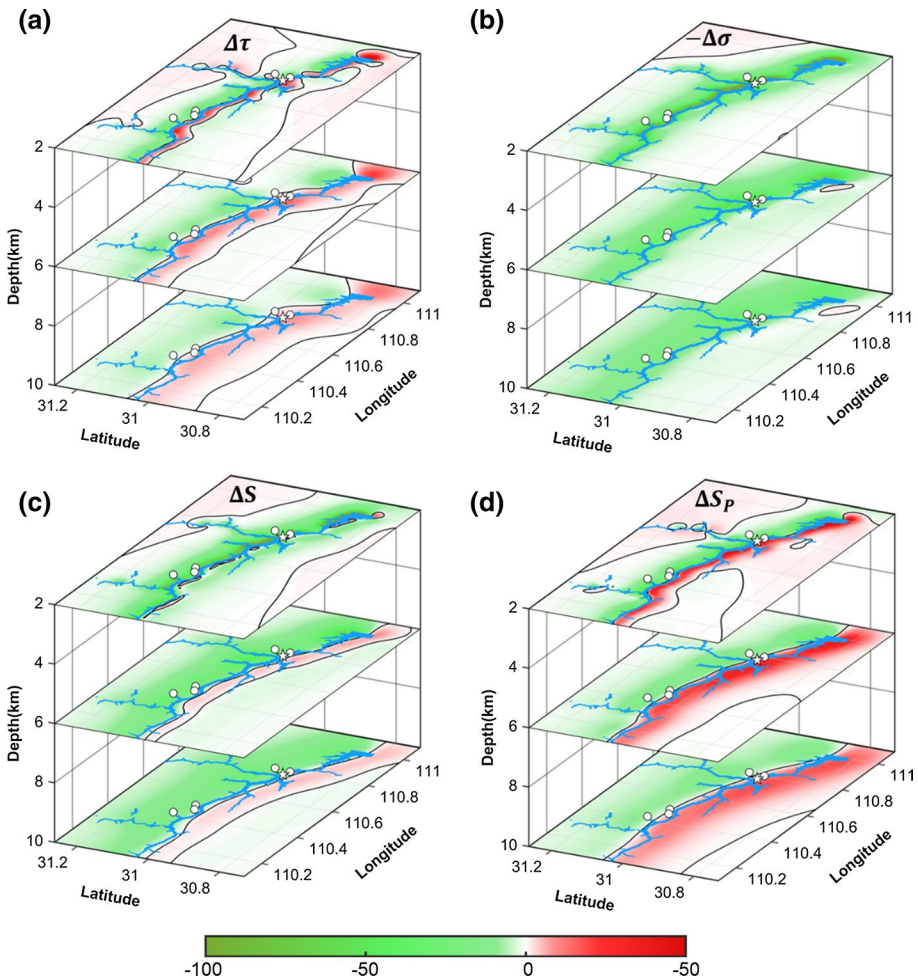
Fig. 5 Same as Fig. 2 but for March 27, 2014 Guojiaba Zone earthquake, having strike = 143°, dip = 60° and rake = 1°

F3 in Fig. 1 and are associated with ambient tectonic stress related frictional failure, as the epicenter of the pre-impoundment earthquake of December 13, 2001 (M 4.5) is also located to the north of the reservoir in this zone (Fig. 1). For the March 27, 2014 type of fault planes, ΔS_P is positive to the south of the reservoir but negative to the north of the reservoir (Figs. 5d, S5 and S6). There is a possibility that these earthquakes are associated with the geological faults, similar to the F2 in Fig. 1 and are triggered by the reservoir impoundment, thereby accounting for the observed increase in the seismic activity to the south of the reservoir. Contradictory results were noticed in the Guoziaba zone earthquakes having March 30, 2014 type of fault plane. In this case, the earthquakes from the region to the north of the reservoir are favoured (as $\Delta \tau$ and ΔS_P are positive) for triggering by the TGR impoundment (Figs. 6, S7 and S8). But negative $\Delta \tau$ (Fig. 6a) and ΔS_P (Figs. 6d, S7 and S8) to the south of the reservoir suggest that the reservoir impoundment is not responsible for the observed increase in the seismic activity in the region to the south of the reservoir for this type of fault planes. There
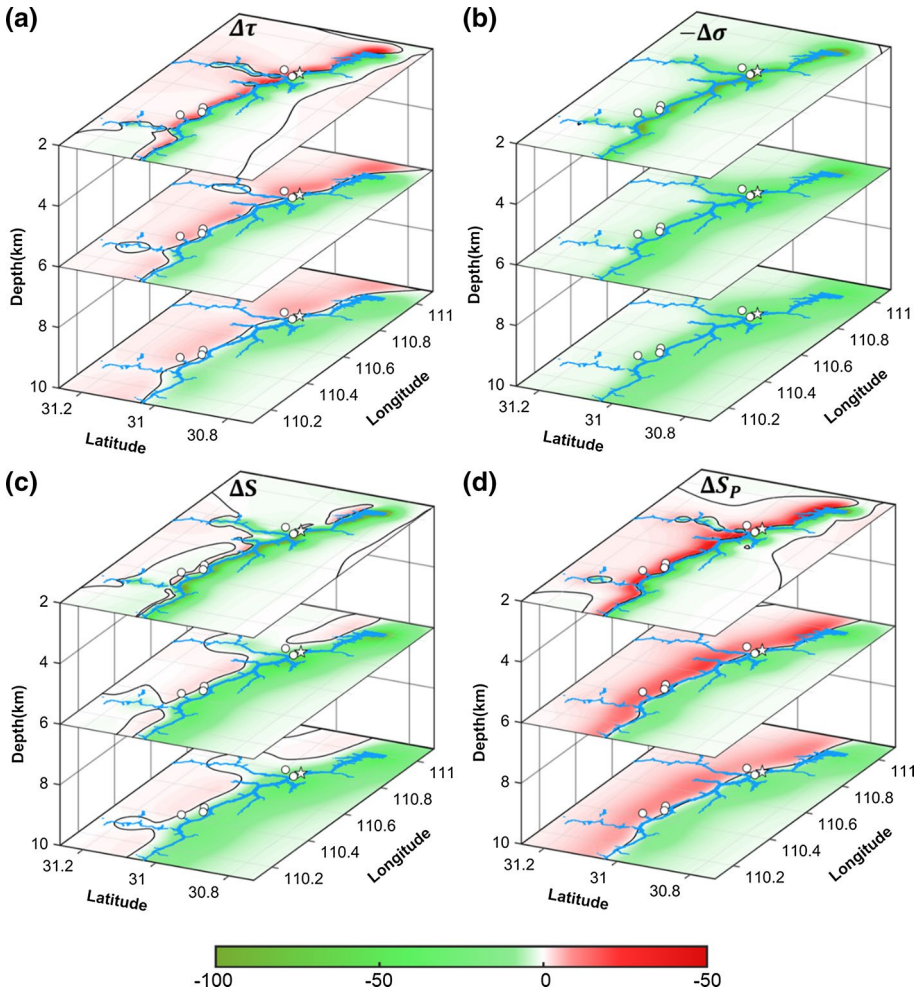
Fig. 6 Same as Fig. 2 but for March 30, 2014 Guojiaba Zone earthquake, having strike = 226°, dip = 54° and rake = 155°

is a possibility that these earthquakes are associated with the geological fault marked as F3 in Fig. 1. In short, Guoziaba zone post-impoundment seismic activity to the north and south of the reservoir can be classified as triggered earthquakes if it occurred on March 30, 2014 and March 27, 2014 type of fault planes, respectively. Seismicity which occurred on November 22, 2008 type of fault plane may be classified as natural tectonic earthquakes, without the influence of the TGR impoundment, or some other factors as discussed below, might have played role in their occurrence.

3.2 Role of other factors in the post-impoundment seismicity of TGR region

Our fault stability analysis indicates that the pore pressure and stress changes induced by the TGR impoundment do not favour shear failure on all seismogenic faults considered
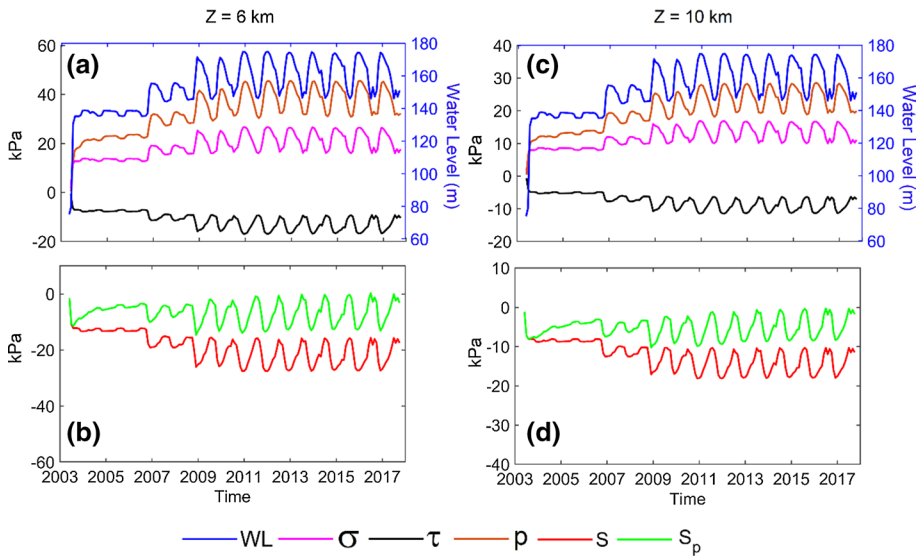
Fig. 7 Temporal variation of $\Delta\tau$, $\Delta\sigma$, ΔP, ΔS and ΔS_{P} with reservoir water level (WL) at the dam site for the same fault plane as considered in Fig. 4 and at the location of November 22, 2008 Guojiaba zone earthquake for $c = 1.0\ \mathrm{m^2/s}$

here. At the same time, there is no doubt that there is an enhancement of seismicity after the TGR impoundment. Thus, the role of other possibilities needs to be assessed critically along with reservoir-assisted shear failure. This prompted us to explore the role of other factors reported in earlier studies. A review article by Chen and Talwani (1998) inferred that in China, large water volume and/or presence of pre-existing faults are not the controlling factors to enhance seismicity after reservoir impoundment which is contrary to the analysis of Simpson (1976) who considered that these two are the important controlling factors in RTS of any region. Chen and Talwani (1998) suggested that the presence of Karst-Carbonate rocks plays a significant role in the RTS cases of China. Based on several observations related to the RTS cases of China, they predicted that the carbonate lithology may assist the occurrence of moderate earthquakes even in the TGR area after its impoundment. Hua (2013) reported that the post-impoundment earthquakes in the TGR region did not follow the traces of faults and fractures, rather they occurred in various clusters (Fig. 3 of Hua et al. 2013). Figure 1 of Zhang et al. (2017) and Fig. 4 of Zhang et al. (2019) also show clustering in post-impoundment earthquakes in the TGR region. These observations are consistent with that of Chen and Talwani (1998) that the presence of active faults is not the controlling factor in the majority of the RTS cases in China. Figure 3 of Hua et al. (2013) and Figs. 2 and 4 of Yi et al. (2012) clearly show that almost all the clusters of post-impoundment earthquakes in the TGR region lie in the Karst-Carbonate located areas. The absence of seismicity in Zigui basin and HLA (Fig. 1), which do not have carbonate rocks, further attests the role of Karst in the occurrence of post-impoundment earthquakes in the TGR region.

If the above mechanism operates in the TGR region then it may be reflected in the earthquake focal mechanisms derived from the full moment tensor inversion. Unfortunately, the majority of the earthquake focal mechanisms are based on double couple solution (Zhang et al. 2016; Yao et al. 2017; Huang et al. 2018) and hence no quantification of isotropic and

non-double couple component have been done. Only in one study (Huang et al. 2019) full moment tensor inversion has been undertaken where predominant double couple component in the focal mechanism has been reported. However, in the absence of detailed information about the number of stations used in the waveform inversion and the fact that these are small magnitude earthquakes, quantification of non-double couple component is a challenge. In such cases, it is important to quantify the deformation using InSAR analysis, estimate the relative contribution of shear and other non-shear components and compare them with the seismic moment released during earthquakes, e.g., as done in Sharma et al. 2020. In the present case, as the rugged topography of the region may cause challenges, we did not attempt it but we hope to do it in the future.

4 Conclusion

Our analysis suggests that enhancement of post-impoundment seismicity in some regions near Three Gorges Reservoir is due to reservoir induced shear failure. In other regions enhanced post-impoundment seismicity is fluid-driven either due to extremely high pore pressure and/or due to the dissolution and collapse of Karst–Carbonate rocks in the area. We also suggest that some larger earthquakes are purely tectonic earthquakes.

Data availability In the supplementary, Tables S1-S2 show the results of fault stability analysis for earthquakes of Three Gorges Reservoir (TGR) region for $z = 2$ km and 6 km. Figures S1–S8 show the results of fault stability analysis for $c = 0.1$ m^2/s and $c = 10$ m^2/s. All data used here are available in previous publications cited in the MS at appropriate places.

Declarations

Conflict of interest The authors declare that they don't have any competing interests.

References

Chen L, Talwani P (1998) Reservoir-induced Seismicity in China. Pure Appl Geophys 153:133–149

Gahalaut K (2021) On the Common Features of Reservoir Water-Level Variations and Their Influence on Earthquake Triggering: An Inherency of Physical Mechanism of Reservoir Triggered Seismicity. Bull Seismol Soc Am. https://doi.org/10.1785/0120200336

Gahalaut K, Gupta PK (2008) An integral equation algorithm for 3-D simulation of pore pressure in a porous elastic medium with heterogeneities. Geophys J Int 175:1245–1253

Hardebeck JL, Nazareth JJ, Hauksson E (1998) The static stress change triggering model: constraints from two southern California aftershock sequences. J Geophys Res 103:24427–24437

Hua W, Zheng S, Yan C, Chen Z (2013) Attenuation, Site Effects, and Source Parameters in the Three Gorges Reservoir Area, China. Bull Seismol Soc Am 103:371–382. https://doi.org/10.1785/0120120076

Huang R, Zhu L, Encarnacion J, Xu Y, Tang C-C, Luo S, Jiang X (2018) Seismic and geologic evidence of water-induced earthquakes in the Three Gorges Reservoir region of China. Geophys Res Lett 45:5929–5936. https://doi.org/10.1029/2018GL077639

Jaeger JC, Cook NGW, Zimmerman RW (2007) Fundamentals of Rock Mechanics. Blackwell Publishing, Oxford, United Kingdom, p 475

Kalpna G, Chander, R. (2000) Green's function based stress diffusion solution in the porous elastic half space for time varying finite reservoir loads. Phys Earth Planet Inter 120:93–101

King GCP, Stein RS, Lin J (1994) Static stress changes and the triggering of earthquakes. Bull Seismol Soc Am 84:935–953

Scholz, C.H. (1990). The Mechanics of Earthquakes and Faulting, Cambridge University Press, 1439 p.

Schorlemmer D, Wiemer S, Wyss M (2005) Variations in earthquake-size distribution across different stress regimes. Nature 437(7058):539–542

Sharma V, Wadhawan M, Rana N, Sreejith KM, Agrawal R, Kamra C, Hosalikar KS, Narkhede KV, Suresh G, Gahalaut VK (2020) A long duration non-volcanic earthquake sequence in the stable continental region of India: The Palghar swarm. Tectonophysics. https://doi.org/10.1016/j.tecto.2020.228376

Simpson DW (1976) Seismicity changes associated with reservoir loading. Eng Geol 10:123–150

Talwani P, Chen L, Gahalaut K (2007) Seismogenic permeability, k_s. J Geophys Res 112:B07309. https://doi.org/10.1029/2006JB004665

Wen-Tao M, Chang-Peng X, Hai-Ou L, Jing-li YUAN, Xi-wei XU, Xin-dong ZHANG, Lan-feng ZHANG (2010) Intensive observation of reservoir-induced earthquake and preliminary analysis on the causes of earthquakes in Three Gorges Reservoir. Seismology and Geology 32:552

Wyss M (1973) Towards a physical understanding of the earthquake frequency distribution. Geophys JR Astron Soc 31(4):341–359

Yao Y, Wang Q, Liao W, Zhang L, Chen J, Li J, Yuan L, Zhao Y (2017) Influences of the Three Gorges Project on seismic activities in the reservoir area. Science Bulletin 62:1089–1098

Yi L, Dong Z, Chenglong L (2012) Preliminary Study of Reservoir-Induced Seismicity in the Three Gorges Reservoir, China. Seism Res Lett. https://doi.org/10.1785/0220110132

Zhang H, Cheng H, Pang Y, Shi Y, Yuen DA (2016) Influence of the impoundment of the Three Gorges Reservoir on the micro-seismicity and the 2013 M5.1 Badong earthquake (Yangtze, China). Phys Earth Planet Inter 261:98–106

Zhang L, Li J, Wei G, Liao W, Wang Q, Xiang C (2017) Analysis of the relationship between water level fluctuation and seismicity in the Three Gorges Reservoir (China). Geodesy and Geodynamics. https://doi.org/10.1016/j.geog.2017.02.004

Zhang L, Li J, Sun X, Liao W, Zhao Y, Wei G, He C (2018) A Possible Mechanism of Reservoir-Induced Earthquakes in the Three Gorges Reservoir, Central China. Bull Seismol Soc Am 108:3016–3028. https://doi.org/10.1785/0120180015

Zhang L, Lei X, Liao W, Li J, Yao Y (2019) Statistical parameters of seismicity induced by the impoundment of the Three Gorges Reservoir, Central China. Bull Seismol Soc Am 103:371–382. https://doi.org/10.1785/0120120076